INTERNATIONAL JOURNAL FOR NUMERICAL METHODS IN FLUIDS, VOL. 24, 693–714 (1997)

AN ALGEBRAIC STRESS FINITE ELEMENT MODEL OF TURBULENT FLOW

J. ALAN ROSS

Consultant, PO Box 4014, #328, Alameda, CA 94501, U.S.A.

AND

BRUCE E. LAROCK

Civil and Environmental Engineering Department, University of California, Davis, CA 95616, U.S.A.

SUMMARY

This paper describes a finite element numerical model for the simulation of both steady and truly transient turbulent flow in two dimensions. All elements of the model and computational approach were chosen, however, for ease of applicability in the future to fully three-dimensional flows. The turbulent mean flow is described by the Reynolds-averaged Navier–Stokes equations. The well-known two-equation $K-\varepsilon$ model is the base for the representation of turbulence quantities. From three candidate algebraic stress models, Rodi's model was chosen for implementation after preliminary tests on turbulent channel flow. The scheme was then tested at length on flow past a backward-facing step and flow past a box. Comparisons were made with the computed and experimental results of other investigators. For the backward-facing step problem the model appears to equal or improve upon the accuracy of predictions of earlier finite element codes. The frequency of vortex shedding from the corners of the box in terms of the Strouhal number is predicted well. © 1997 by John Wiley & Sons, Ltd.

KEY WORDS: finite element; turbulence; algebraic stress model

INTRODUCTION

The numerical simulation of any transient turbulent flow attempts to overcome several difficult problems. The convective acceleration term in the Reynolds-averaged form of the equation for conservation of linear momentum are non-linear, and the use of any but the simplest eddy viscosity model of turbulent transport will introduce additional non-linearities and coupling between the mean flow equations and the turbulence model itself. Moreover, many turbulent flows possess features that absolutely require a time-dependent computation; the generation and shedding of vortices from the corners of solid objects in the flow are only one such example. Although most work in past years on such problems has been based on finite difference methods, the present effort is finite-element-based.

This paper will describe progress towards the long-term goal of developing a three-dimensional finite element code for the simulation of transient turbulent flows, although the focus of this paper will be on a two-dimensional implementation and testing of the algorithm. The mean flow model is based on the Reynolds-averaged Navier–Stokes equations, also called simply the Reynolds equations, for incompressible flow. The Reynolds stress terms could be modelled by the two-equation $K-\varepsilon$ model, and this was done at an intermediate stage of the development. However, this model was in

CCC 0271–2091/97/070693–22 $17.50

Received 22 March 1995
Revised 9 July 1996

the end augmented by an algebraic stress model chosen from three candidate models. This step was taken to separate the values of the turbulent normal stresses; as is well known, this feature is essential in the representation of flows such as turbulent flow in a rectangular duct. Rodi's algebraic stress model (ASM) was chosen for use in this project. The code was tested extensively in simulating turbulent flow past a backward-facing step and around a square cylinder or box; in both examples the code was quite successful in simulating the features of these flows.

MEAN FLOW AND TURBULENCE MODEL EQUATIONS

The Reynolds decomposition was used to develop the mean flow equations for conservation of mass and linear momentum for an incompressible fluid. They are

$$\frac{\partial U_i}{\partial x_i} = 0 \tag{1}$$

and

$$\frac{\partial U_i}{\partial t} + U_j \frac{\partial U_i}{\partial x_j} = -\frac{\partial P}{\partial x_i} + \frac{\partial}{\partial x_j}\left[\nu \left(\frac{\partial U_i}{\partial x_j} + \frac{\partial U_j}{\partial x_i} \right) - \overline{u_i u_j} \right], \tag{2}$$

where U_i is the time-averaged mean flow velocity component, u_i is the fluctuating velocity component, P is the mean flow pressure divided by the density, t is time, x_i is the Cartesian coordinate direction, ν is the fluid kinematic viscosity and $-\overline{u_i u_j}$ is the Reynolds stress per unit mass. In all equations the Einstein convention is used, wherein a repeated subscript within a term implies summation over the full subscript range.

In equations (1) and (2) one can clearly see that the number of fluid variables exceeds the number of equations. To achieve closure of this equation set, one must make assumptions about the nature of the turbulent flow. Each different closure is called a turbulence model; many such models exist, but most fit into only a few categories.

The K–ε model,[1] which employs the eddy viscosity concept, forms the base of the turbulence representation that will be used in this project. In principle the processes of turbulence production, dissipation, redistribution and diffusive transport are all present in any model variant that is built on this base representation; here it will be augmented by an algebraic stress model to separate the normal stresses. The constitutive law that introduces the eddy viscosity concept is

$$-\overline{u_i u_j} = 2\nu_t D_{ij} - \tfrac{2}{3} K \delta_{ij}, \tag{3}$$

in which $K = \overline{u_i u_i}/2$ is the turbulence kinetic energy per unit mass, ν_t is the kinematic eddy viscosity and D_{ij} is the mean rate-of-strain tensor defined by

$$D_{ij} = \frac{1}{2}\left(\frac{\partial U_i}{\partial x_j} + \frac{\partial U_j}{\partial x_i} \right). \tag{4}$$

The kinematic eddy viscosity can, using dimensional analysis, be expressed in terms of K and the energy dissipation rate ε in the form

$$\nu_t = c_\mu \frac{K^2}{\varepsilon}. \tag{5}$$

Then the distribution of the scalar turbulence parameters K and ε over the flow domain is described by two semi-empirical transport equations which complete the $K-\varepsilon$ model:

$$\frac{\mathrm{D}K}{\mathrm{D}t} = \frac{\partial}{\partial x_i}\left(\frac{v_\mathrm{t}}{\sigma_K}\frac{\partial K}{\partial x_i}\right) + G - \varepsilon, \tag{6}$$

$$\frac{\mathrm{D}\varepsilon}{\mathrm{D}t} = \frac{\partial}{\partial x_i}\left(\frac{v_\mathrm{t}}{\sigma_\varepsilon}\frac{\partial \varepsilon}{\partial x_i}\right) + c_{\varepsilon 1}\frac{\varepsilon}{K}G - c_{\varepsilon 2}\frac{\varepsilon^2}{K}, \tag{7}$$

in which

$$G = -\overline{u_i u_j}\frac{\partial U_i}{\partial x_j} = 2v_\mathrm{t}D_{ij}\frac{\partial U_i}{\partial x_j} \tag{8}$$

is the production of turbulence by the mean-flow shear. In these equations $\mathrm{D}/\mathrm{D}t$ is the material derivative. In equation (6) the transport of K is influenced by terms representing diffusive transport, turbulence production by the mean-flow shear and by the dissipation rate ε. In equation (7) the transport of ε is modelled in terms of diffusive transport, source and sink terms on the right. The empirical constants take the standard values[1] $c_\mu = 0{\cdot}09$, $c_{\varepsilon 1} = 1{\cdot}44$, $c_{\varepsilon 2} = 1{\cdot}92$, $\sigma_K = 1{\cdot}0$ and $\sigma_\varepsilon = 1{\cdot}3$.

To model the individual Reynolds stresses without resorting to the use of additional partial differential equations, researchers have created algebraic stress models; these augment the two $K-\varepsilon$ transport equations with a constitutive model that does not require an additional partial differential equation for each individual stress component. Over a half dozen such models have been proposed since Rodi proposed the first of these models.

This research investigated three models developed by Rodi,[2] Speziale[3] and Ahmadi and Chowdhury.[4] Rodi's final constitutive equation is

$$\overline{u_i u_j} = \tfrac{2}{3}K\delta_{ij} + \frac{K(1-c_{a2})}{c_{a1} + G/\varepsilon - 1}\left(\frac{S_{ij}}{\varepsilon} - \frac{2}{3}\frac{G}{\varepsilon}\delta_{ij}\right), \tag{9}$$

with

$$S_{ij} = -\overline{u_i u_k}\frac{\partial U_j}{\partial x_k} - \overline{u_j u_k}\frac{\partial U_i}{\partial x_k} \tag{10}$$

and the coefficients[5] $c_{a1} = 2{\cdot}5$ and $c_{a2} = 0{\cdot}55$. From equation (8) one sees that Rodi's model, equation (9), is non-linear in the Reynolds stresses; comments on the treatment of this feature will be found in two places later in the paper. Speziale's stress model[6] is

$$\overline{u_i u_j} = \tfrac{2}{3}K\delta_{ij} - 2v_\mathrm{t}D_{ij} - \frac{4C_\mathrm{D}v_\mathrm{t}^2}{K}(D_{im}D_{mj} - \tfrac{1}{3}D_{mn}D_{mn}\delta_{ij}) - \frac{4C_\mathrm{E}v_\mathrm{t}^2}{K}(\tilde{D}_{ij} - \tfrac{1}{3}\tilde{D}_{mm}\delta_{ij}), \tag{11}$$

in which $\tilde{D}_{ij}$ is the Oldroyd derivative defined by

$$\tilde{D}_{ij} = \frac{\partial D_{ij}}{\partial t} + U_k\frac{\partial D_{ij}}{\partial x_k} - \frac{\partial U_i}{\partial x_m}D_{mj} - \frac{\partial U_j}{\partial x_m}D_{mi} \tag{12}$$

and $C_\mathrm{D} = C_\mathrm{E} = 1{\cdot}68$. Ahmadi's model[4] describes the Reynolds stresses as

$$\overline{u_i u_j} = \tfrac{2}{3}K\delta_{ij} - 2v_\mathrm{t}D_{ij} - \frac{av_\mathrm{t}K}{\varepsilon}\left(\frac{\hat{\mathrm{D}}(D_{ij})}{\mathrm{D}t} + \frac{1}{v_\mathrm{t}}D_{ij}\frac{\mathrm{D}v_\mathrm{t}}{\mathrm{D}t}\right) + \frac{\beta v_\mathrm{t}K}{\varepsilon}(D_{ik}D_{jk} - \tfrac{1}{3}D_{mn}D_{mn}\delta_{ij}), \tag{13}$$

in which the Jaumann derivative and vorticity are respectively

$$\frac{\hat{\mathrm{D}}(D_{ij})}{\mathrm{D}t} = \frac{\mathrm{D}(D_{ij})}{\mathrm{D}t} + D_{ik}\Omega_{kj} + D_{jk}\Omega_{ki}, \qquad \Omega_{ij} = \frac{1}{2}\left(\frac{\partial U_i}{\partial x_j} - \frac{\partial U_j}{\partial x_i}\right), \tag{14}$$

with $a = 0{\cdot}93$ and $\beta = 0{\cdot}54$ for flow near a wall. These last two models both contain many more terms than Rodi's model but are linear in the Reynolds stresses; in contrast, they are highly non-linear in K and ε via the eddy viscosity itself. An early objective of this research was to compare the performance of these three models for a standard flow using the present numerical modelling techniques and to select one model for further use.

NUMERICAL MODELLING TECHNIQUES

After a preliminary screening of algorithmic choices, it was decided to pattern this numerical solution after the work of Gresho *et al.*,[7] who developed an efficient transient code for laminar flows, in their general approach to computations. A reading of the 40 pages of Reference 7 will explain much about the features of this approach, so this section will simply describe the primary features of this implementation and also emphasize some differences. This modified finite element method was first applied to turbulent flows by Haroutunian,[8] who used a $K-\varepsilon$ model to describe the turbulence parameters. Reference 9 also supplies much additional detail on these techniques. In this method the individual element representations of the unknowns are simple, and the basic time integration scheme is also very simple but fast. However, accuracy in integration is still retained by using the balancing tensor diffusivity approach, as Gresho *et al.*[7] explain. While this paper discusses only two-dimensional examples and uses only quadrilateral elements, these computational techniques are carefully chosen to be also applicable directly to three-dimensional problems and additional element shapes. Moreover, the solution strategy is actually best suited for the simulation of flows which are inherently transient and have no steady flow analogue.

The basic approach is a modified Galerkin finite element method. Here the Galerkin method spatially discretizes the partial differential equations of transient flow into a system of ordinary differential equations, which is then integrated in time using the explicit forward Euler technique. The spatial numerical integration process used one-point Gaussian quadrature, which is accurate for all terms with the exception of the diffusion terms. The inaccuracies were corrected by adding an 'hour-glass' correction term.[7] The continuity constraint is satisfied at every time by computing pressures from a Poisson equation for the modified pressure $\hat{P} = P + 2K/3$. The Poisson equation is derived from the original momentum and continuity equations. The resulting modified pressure matrix is symmetric, thus requiring one to store only the upper triangular terms. The matrix entries depend only on the mesh topology, so the matrix must be inverted only once and then stored. The modified pressure and the pressure itself are then found by a direct back substitution.

The mean flow velocity components and also K and ε are all interpolated linearly, but the modified pressure is piecewise constant within an element; the Galerkin weighting of the Reynolds, K and ε equations is also linear. In all equations the second-order diffusive terms are integrated once by parts.

The explicit forward Euler method is used for time integration. As is well known, this approach is destabilizing because of the numerical diffusion that is created, especially in convection-dominated flows. The balancing tensor diffusivity scheme[7] is used to counter this false, negative diffusion for both the mean flow and the $K-\varepsilon$ model variables. The net effect is to add locally a term of the form $U_i U_j \Delta t/2$ to the usual coefficient of the diffusive term. In addition, the $K-\varepsilon$ model time integration scheme is modified somewhat to make it actually semi-implicit.[9]

The Rodi ASM is an implicit model, since the individual stresses appear on both sides of the model equations. Various kinds of solution procedures for these equations have in the past led to divergent computations. After some searching, two computational steps were found to produce a fast, simple algorithm which does not blow up. The first step is simply to evaluate the stresses on the right side of the ASM equations at the beginning of each time step (i.e. lagging them by one time step), avoiding iterations and taking advantage of the fact that the individual time steps are small. The second step is to set an upper limit on the allowable magnitude of the source terms in the ASM and locally 'clip' any source terms which exceed the limit. More will be said about this 'clipping' in the section on examples.

The boundary and initial conditions for each problem will be described with the problems.

EXAMPLES AND DISCUSSION

The first tests[9] of this finite element code checked to verify that the algorithm, without the turbulence model, could simulate laminar flows properly. Turbulent channel flow[9,10] was then used, as has been previously reported,[10] as a test problem both to check further the basic algorithm and to compare the performance of the three different algebraic stress models.

In this section some results of extensive code testing for turbulent flow over a backward-facing step will be described. Then new results will be presented for turbulent flow around a square box. In this work some computations employed up to 4004 nodes and a proportional number of time steps.

The codes for this project were developed in Pascal to take advantage of compiler features, but the graphics codes were developed in Fortran to use Fortran library routines to drive a Tektronix terminal emulator. A more efficiently executing production code could have been produced in Fortran, but the code would have required many more statements. Such a Fortran code was not written, and it is the authors' opinion that run statistics from the Pascal code might not be representative of the efficiencies that could be achieved via these methods. Also, to check the progress of computations, some executions were periodically halted and later restarted; these restarts had a noticeable but not easily quantifiable effect on overall CPU time and on the number of time steps in a solution. Storage requirements were not large; for example, for all examples the solutions of the symmetric, banded pressure matrix were completed in core.

Results from the fully developed channel flow problem

The governing equations for this problem are essentially diffusion equations. The ASMs and the $K-\varepsilon$ model itself lead to continuum equations that are identical, but the numerical procedures are not quite the same. For all variants of this problem, two-dimensional elements were tested, although the problem did not require their use. It must be remarked that none of these particular algebraic stress models was constructed specifically for flow in the proximity of a wall; other models, or even other versions of some of these models, could perform better in this particular comparison. However, it was felt that this test comparison was an impartial comparison precisely because none of the models was specially developed for the test problem.

In applying just the $K-\varepsilon$ model, once calculates the gradient of the mean velocity and the kinematic eddy viscosity directly. In applying the algebraic stress models, the Reynolds stress was first computed at the element centroids; then these values were smoothed to the element nodes, and finally the gradients of Reynolds stress were computed from these smoothed values. Testing this computational sequence was a precursor to the application of the ASM to the other two problems.

For turbulent channel flow the algebraic stress models predict somewhat differing stress relations. As Schamber[11] has shown, the Rodi model predicts

$$\overline{uu} = 0{\cdot}94K, \qquad \overline{vv} = \overline{ww} = 0{\cdot}53K, \qquad \overline{uv} = -0{\cdot}33K. \tag{15}$$

Speziale's model[6] predicts

$$\overline{uu} = -\tfrac{2}{3}K + 0{\cdot}352\frac{v_t K}{\varepsilon}\left(\frac{dU}{dy}\right)^2, \tag{16a}$$

$$\overline{vv} = -\tfrac{2}{3}K - 0{\cdot}252\frac{v_t K}{\varepsilon}\left(\frac{dU}{dy}\right)^2, \tag{16b}$$

$$\overline{ww} = -\tfrac{2}{3}K - 0{\cdot}100\frac{v_t K}{\varepsilon}\left(\frac{dU}{dy}\right)^2, \tag{16c}$$

$$\overline{uv} = -v_t\frac{dU}{dy}, \tag{16d}$$

while Ahmadi's model[4] predicts the Reynolds stresses as

$$\overline{uu} = -\tfrac{2}{3}K + 0{\cdot}51\frac{v_t K}{\varepsilon}\left(\frac{dU}{dy}\right)^2, \tag{17a}$$

$$\overline{vv} = -\tfrac{2}{3}K - 0{\cdot}42\frac{v_t K}{\varepsilon}\left(\frac{dU}{dy}\right)^2, \tag{17b}$$

$$\overline{ww} = -\tfrac{2}{3}K - 0{\cdot}09\frac{v_t K}{\varepsilon}\left(\frac{dU}{dy}\right)^2, \tag{17c}$$

$$\overline{uv} = -v_t\frac{dU}{dy}. \tag{17d}$$

For the channel flows there is clearly no difficulty in representing the individual stresses with linear elements. Results for profiles of mean velocity, turbulence kinetic energy and Reynolds stress were all obtained from the $K-\varepsilon$ model and from the ASMs;[9,10] they were carefully compared with data from References 12–14. The results are judged to be very good and are in agreement with those of other numerical investigators.[8,15]

A limited selection of the results of these computational tests is shown in Figures 1–4. In Figure 1 non-dimensional mean velocity profiles are presented for the $K-\varepsilon$ and algebraic stress models and compared with Laufer's experimental data. (Speziale's profile matched Ahmadi's profile and is not shown.) While all models do rather well, Rodi's profile compares best with Laufer's data, and the other computed profiles are about 2 per cent low. In the next three figures the individual non-dimensional normal Reynolds stress components are compared with the experimental data of Laufer and Clark. In Figure 2 one sees the separation of normal Reynolds stresses with qualitatively good comparisons with Laufer's data for Rodi's ASM. One sees in Figure 3 that the three normal Reynolds stresses are all separated by Speziale's ASM; the shapes of the curves compare well with Laufer's data, but the numerical values are high. For the channel flow problem this model produces the best Reynolds stress comparisons. In Figure 4 Ahmadi's ASM separates the normal stresses with $\overline{uu} > \overline{ww} > \overline{vv}$, but the shape of the $\overline{vv}$ profile is incorrect. The $\overline{uu}$ and $\overline{ww}$ profile shapes match Laufer's data well, but the numerical values are too high and too low respectively. After comparisons were completed, the overall results predicted by Rodi's ASM were judged to match Laufer's stress

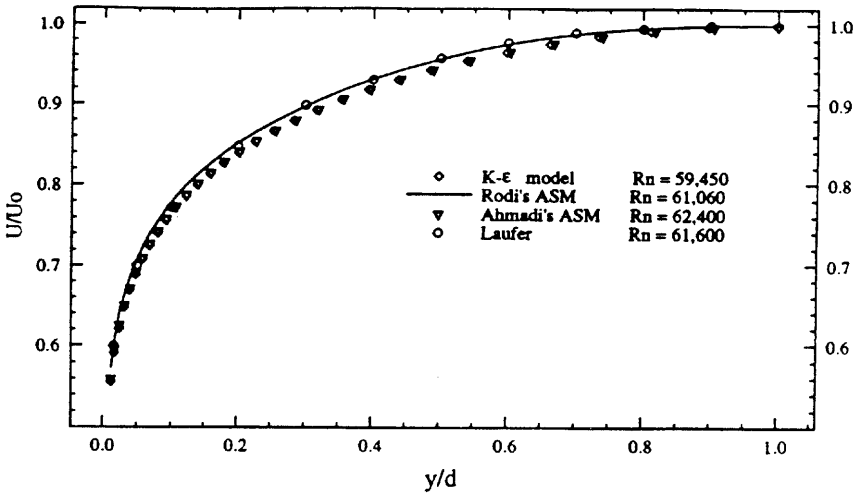

Figure 1. Mean flow velocity profiles for half-channel. Rodi's ASM closely matched Laufer's profile. Speziale's ASM matched the profile from Ahmadi's ASM and is not shown

data better than the results from the other two models, especially when the relative simplicity of this model is considered, and Rodi's ASM was then selected for further use.

Flow over a backward-facing step

This problem has served as a benchmark for experimentalists and numerical studies for years. At least seven previous numerical and eight experimental investigations of this turbulent flow problem have been conducted.[9] This work will compare present predictions primarily with the experimental results of Kim[16] and the numerical results of Haroutunian.[8] Figure 5 is a schematic diagram (note

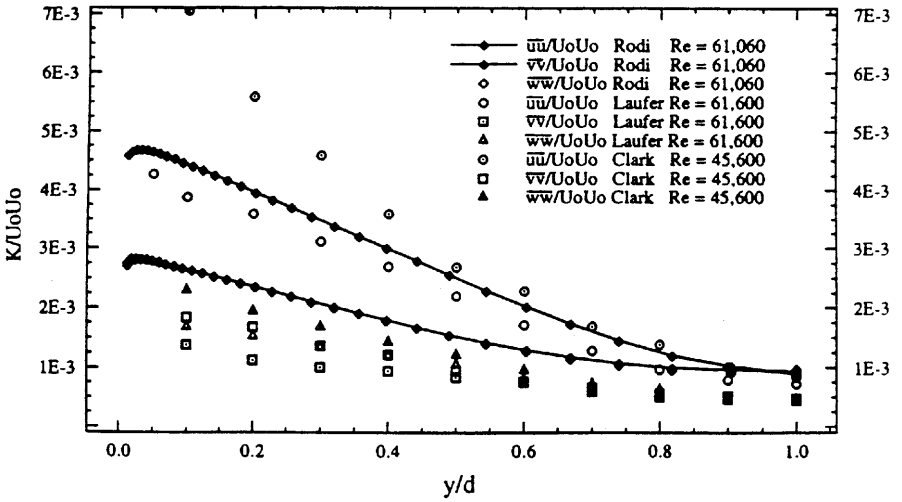

Figure 2. Non-dimensional normal Reynolds stress profiles for half-channel, according to Rodi's ASM. Comparisons are made with the experimental data of Laufer and Clark. Rodi's $\overline{vv}$ and $\overline{ww}$ components are the same

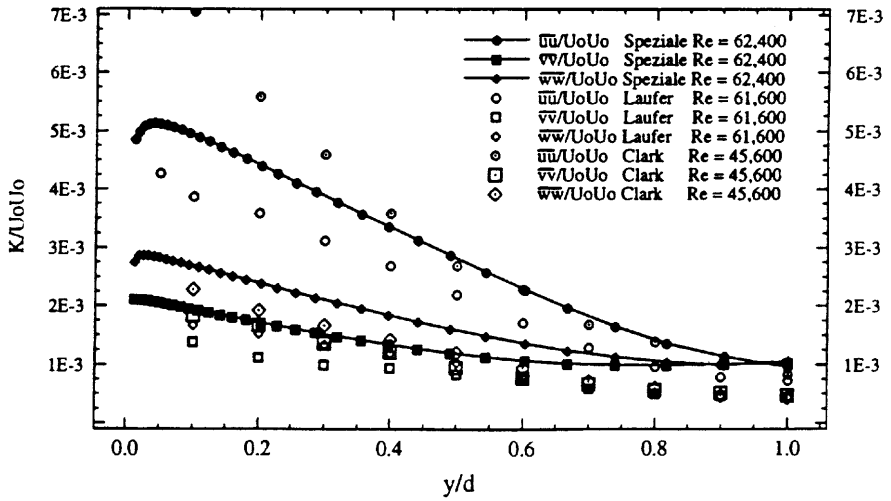

Figure 3. Non-dimensional normal Reynolds stress profiles for half-channel, according to Speziale's ASM. This model produced the best normal stress comparisons with the experimental normal stress data of Laufer and Clark

scales on the figure) of the basic mesh and boundary conditions for a step increase in duct width from $2H$ to $3H$, where H is the step height; the mesh is 43 by 67 nodes, including 288 which are zeroed out within the step. Along wall boundaries u^* and ε are

$$u^* = \frac{\kappa U_W}{\ln[Ey_n(c_\mu^{1/2}K)^{1/2}/\nu]}, \qquad \varepsilon = \frac{(c_\mu^{1/2}K)^{3/2}}{\kappa y_n}, \tag{18}$$

in which U_W is the wall velocity, $\kappa = 0{\cdot}40$ is the von Kármán constant, y_n is the stand-off distance from each solid wall to the edge of the computational mesh, chosen so that $30 \leqslant u^* y_n/\nu \leqslant 100$, and E

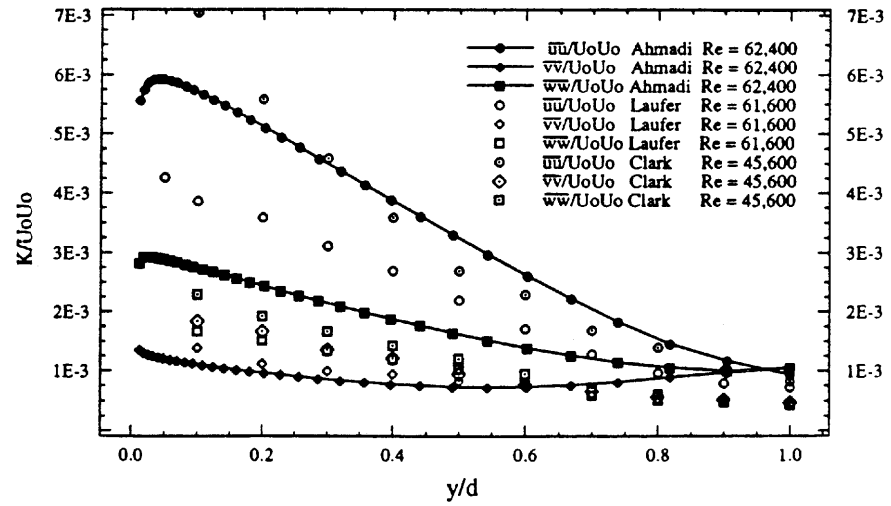

Figure 4. Non-dimensional normal Reynolds stress profiles for half-channel, according to Ahmadi's ASM. Comparisons are made with the experimental data of Laufer and Clark. The normal stresses are separated, but values of $\overline{uu}$ and $\overline{vv}$ are respectively higher and lower than Laufer's data

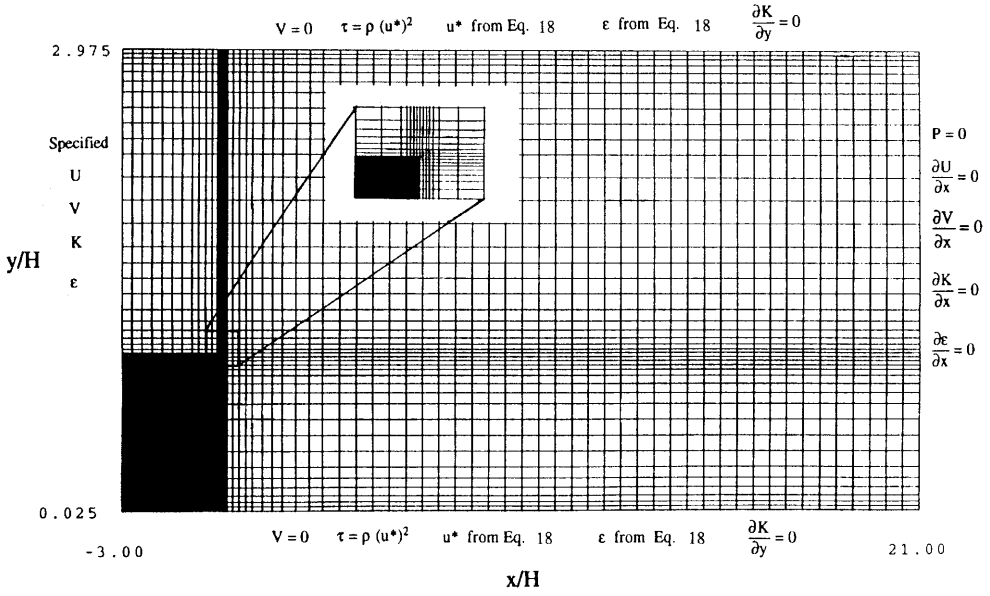

Figure 5. Backward-facing step mesh and boundary conditions. Additional boundary conditions are $V = 0$ atop the step and $U = 0$ on the vertical side; K and ε are as for other solid boundaries

is a constant which depends on the wall smoothness. In this case $y_n/H = 0{\cdot}025$. Inlet section data were obtained from the fully developed channel flow problem. The transient simulation could in principle be initialized with any divergence-free velocity field.[7] All other boundary conditions for this flow are shown in Figure 5 itself.

A typical streamline plot is presented in Figure 6 for flow at a Reynolds number of 47,000 based on the step height and maximum inlet velocity; if the Reynolds number were based on the mean inlet velocity, it would be somewhat lower. Results in this particular figure were computed with the $K-\varepsilon$ model itself, and the computed separation length, i.e. the distance along the lower wall from the step to the intersection of the zero streamline, was $y/H = 6{\cdot}7$, which compares well with Kim's experimental value of $7{\cdot}0 \pm 1{\cdot}0$. As with first eight rows of Table I show, this prediction compares better with Kim's measurement than do the predictions of almost all other numerically based $K-\varepsilon$ codes (all entries in the table are for a Reynolds number of 45,000 except the present work). In this computation the Reynolds stresses were computed at the element level and then smoothed to the nodes at each time step. The source term G was computed from velocity gradients at the element centroids. Then the nodal Reynolds stresses were averaged to obtain the subsequent centroidal values. This process had the effect of making the computed separation longer. When the Reynolds stresses were computed at the element centroids and not redistributed to the nodes, as is done when using the algebraic stress model to reduce computing costs, the predicted separation zone length changed to about 6·3, which is almost identical with Haroutunian's result. Only two other reports of separation lengths above 6·0 appear. Thangan and Speziale report the need to use a special wall model to achieve their value of 6·25, while Lee's work, like Kim's experiment, has a flatter than normal velocity profile at the entrance, leading to longer separation regions.

When the flow field was computed with the ASM, the resulting separation length was 6·6, which again compares favourably with similar entries in Table I. Early computations with this numerical scheme failed, however, apparently owing to a feedback between mean flow velocity gradients and

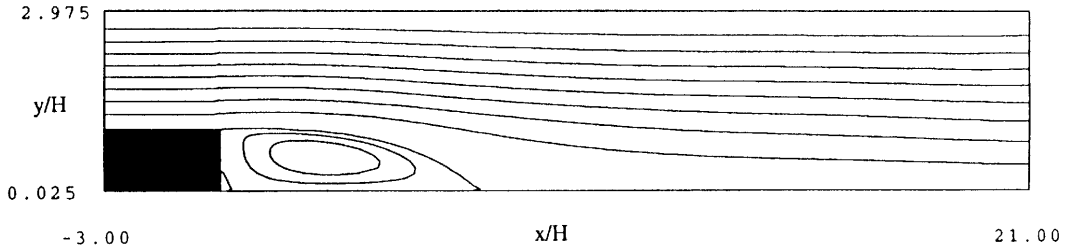

Figure 6. Streamlines for backward-facing step

turbulence model source/sink terms. A remedy for this problem without resorting to upwinding or the direct addition of more numerical diffusion was sought; eventually it was discovered that a simple restriction on the magnitude of the ASM source terms, called 'clipping', led to a successful, stable result. This process was actually employed less than 20% of the time during computations and never involved more than 16 nodes (less than 1% of the nodes in the field), all immediately downstream of the nose of the step where the shear is greatest. Local mesh refinement, a common remedy for this kind of problem, may not be a solution, since this would produce still shorter distances between nodes and could enhance the intensity of local gradients.

The 'clipping' process, in addition to being a way to stabilize computations, is related to the desire to create a code that could easily switch between the solution of the $K-\varepsilon$ model and the ASM. First the momentum equation (2) was rewritten in the form

$$\frac{\partial U_i}{\partial t} + U_j \frac{\partial U_i}{\partial x_j} = -\frac{\partial P}{\partial x_i} + \frac{\partial}{\partial x_j}\left[(\nu + \nu_t)\left(\frac{\partial U_i}{\partial x_j} + \frac{\partial U_j}{\partial x_i}\right)\right] + R_i, \tag{19}$$

with

$$R_i = \left|\frac{\partial}{\partial x_j}(\overline{u_i u_j})\right|_{K-\varepsilon} - \left|\frac{\partial}{\partial x_j}(\overline{u_i u_j})\right|_{\mathrm{ASM}}. \tag{20}$$

This last term is the difference in an individual Reynolds stress per unit mass between the predictions of the $K-\varepsilon$ model and the (Rodi) ASM. The stress terms were bilinearly discretized over an element,

Table I. Separation lengths for backward-facing step

Investigator	Approach	Separation length L/H
Kim[16]	Experiment	$7{\cdot}0 \pm 1{\cdot}0$
This work	$K-\varepsilon$	6·3–6·7
Betts and Haroutunian[17]	$K-\varepsilon$	6·25
Haroutunian[8]	$K-\varepsilon$	6·3
Speziale and Ngo[6]	$K-\varepsilon$	5·5
Thangam and Speziale[18]	$K-\varepsilon$	6·0
With wall model	$K-\varepsilon$	6·25
Lee[19]	$K-\varepsilon$	7·1
This work	ASM	6·6
Speziale and Ngo[6]	ASM	6·4
Ahmadi and Chaudhury[4]	ASM	6·5
Thangam and Speziale[18]	ASM	6·8

the rest of the discretization process being as described earlier, and with a few binary switches the computer code could move from one model to the other. The 'clipping' was a limitation on the size of R_i. The clipping level of $5{\cdot}0\,6\,10^{74}$ (units are m s^{72}) was chosen by running the code for a few time steps and noting that the magnitude of the source term R_i was about $1{\cdot}0\,6\,10^{74}$. In fact, this clipping level worked so well that no additional experimentation with the level of clipping was done.

A contour plot of the normalized turbulence kinetic energy per unit mass, K/U_0^2, predicted by the $K-\varepsilon$ model is presented in Figure 7. It shows a single maximum of 0·045 located about five step heights downstream of the step. With the ASM the contours are very similar, with a single maximum of 0·043 at six step heights downstream. Interestingly, Haroutunian[8,17] shows two maxima of 0·041 at five step heights downstream and immediately downstream of the step. The present work also predicts two maxima (magnitudes 0·041 and 0·071) at the same locations when in the computations the Reynolds stresses were computed at the element centroids and not redistributed to the nodes. A contour plot of the normalized dissipation rate $\varepsilon/(U_0^3/H)$ is indistinguishable from that of Haroutunian[8] and is not presented here.

The value of the ASM computation in relation to the analogous $K-\varepsilon$ computation can be seen most clearly in contour plots of the (negative of the) normalized Reynolds stresses per unit mass, $\overline{uu}/U_0^2$, $\overline{vv}U_0^2$ and $\overline{uv}/U_0^2$, in Figures 8–10, computed with the ASM. In any $K-\varepsilon$ prediction the normal stresses must be the same, but an ASM separates the individual values. In Figure 8 the maximum value of $\overline{uu}/U_0^2$ is 0·041 at $x/H = 5{\cdot}5$, whereas the $K-\varepsilon$ model predicts a maximum of 0·03 at $x/H = 5{\cdot}8$ and Eton[20] measured a maximum of about 0·045. In Figure 9 the maximum value of $\overline{vv}/U_0^2$ is 0·024 at $x/H = 5{\cdot}6$, which is lower than the other normal stress component by about 25%. The shear stress contours, Figure 10, are quite similar to the result of the $K-\varepsilon$ computation but somewhat higher. Ross[9] presents an additional 30 or so plots of results for this problem.

Kim's experiments on this flow developed profiles of the horizontal velocity and Reynolds stresses at various sections downstream of the step. Figures 11–15 compare these experimental results with corresponding results from computations for the $K-\varepsilon$ model and the ASM model.

The normalized horizontal velocity profiles, Figure 11, generally indicate that the results from the $K-\varepsilon$ model differ little from the ASM results, and both match the experimental results reasonably well near the step at $x/H = 1{\cdot}5$ and 2·6 (x is the horizontal distance and H is the step height). The inlet conditions for Kim's experiment generated a flatter inlet velocity profile which in turn created higher horizontal velocity components, indicated by the profiles, than are predicted by the uniform channel flow used in this study. The separation length calculated with both the $K-\varepsilon$ model and the ASM could probably have been increased by using a flatter inlet velocity profile. Further downstream at $x/H = 5{\cdot}5$ both turbulence models underpredict the negative horizontal velocity components along the wall, which is associated with the shorter calculated circulation zone. At section $x/H = 10{\cdot}5$ the

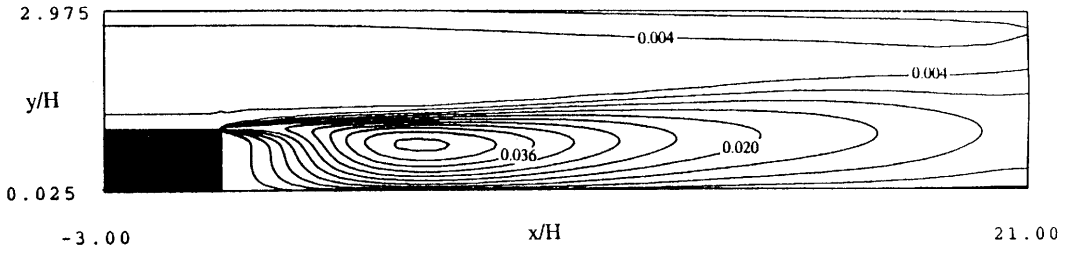

Figure 7. Contour plot of non-dimensional turbulence kinetic energy per unit mass, K/U_0^2, contour interval 0·004, for flow over backward-facing step

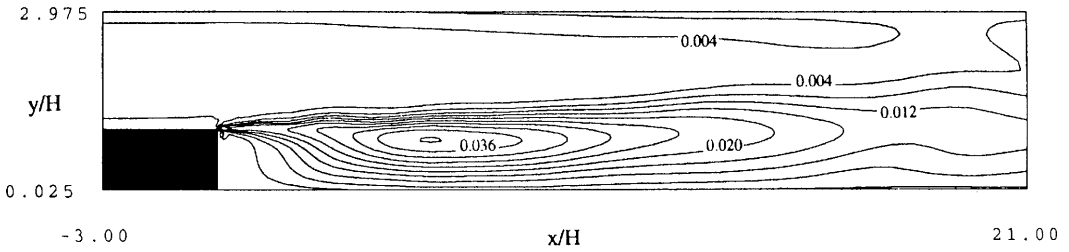

Figure 8. Contour plot of non-dimensional normal Reynolds stress $\overline{uu}/U_0^2$, contour interval 0·004, for flow over backward-facing step

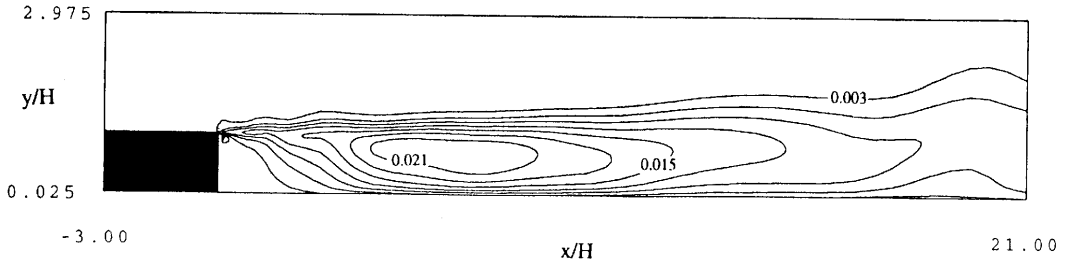

Figure 9. Contour plot of non-dimensional normal Reynolds stress per unit mass, $\overline{vv}/U_0^2$, contour interval 0·003, for flow over backward-facing step

experimental data indicate that the velocity is returning to a normal channel flow distribution sooner than is predicted by either computational model.

Comparisons of the normal Reynolds stresses at several sections downstream of the step are shown in Figures 12–14. These profiles clearly show that the ASM distinctly separates the magnitudes of the horizontal and vertical stress components, while the $K-\varepsilon$ model does not do so. At the sections closer to the step (x/H from 4·0 to 10·5) the normal Reynolds stresses predicted by the ASM more closely match the experimental data than do the predictions of the $K-\varepsilon$ model. Further downstream at sections x/H of 13·5 and 15·5 the normal Reynolds stresses $\overline{uu}/U_0^2$ are overpredicted by the ASM and underpredicted by the $K-\varepsilon$ model. The Reynolds stresses $\overline{vv}/U_0^2$ predicted by both models are nearly identical and closely match the experimental data. The magnitudes of the horizontal and vertical normal stresses from the $K-\varepsilon$ model are almost identical. This means that the normal stresses for the

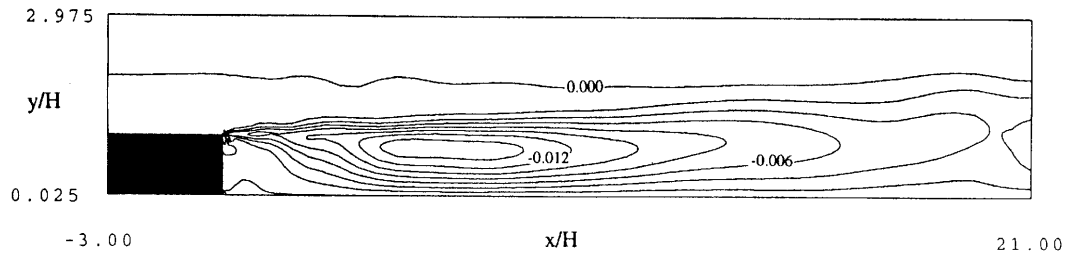

Figure 10. Non-dimensional contour plot of $\overline{uv}/U_0^2$, contour interval 0·002, for flow over backward-facing step

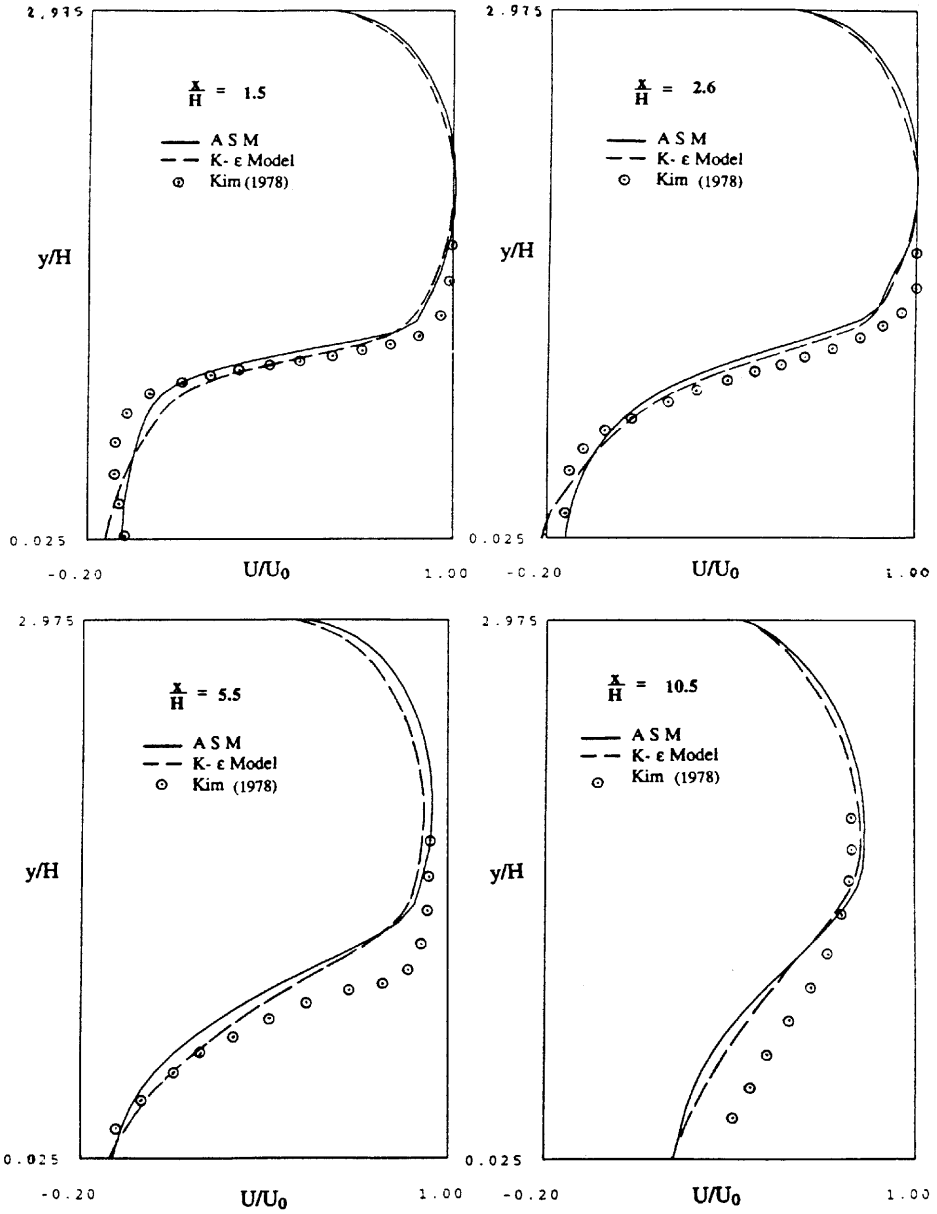

Figure 11. Comparison of mean horizontal velocity profiles U/U_0 at various locations downstream of step. The maximum inlet velocity is U_0 and H is the step height. The experimental data are taken from Reference 16

$K-\varepsilon$ model from equation (3) are more dependent upon the turbulence kinetic energy than on the gradients of the velocity.

The shear stress profiles are shown in Figure 15. The ASM predictions of shear stress are closer to the experimental data in the zones of high shear downstream of the step. Further downstream both the ASM and the $K-\varepsilon$ model overpredict the shear stress.

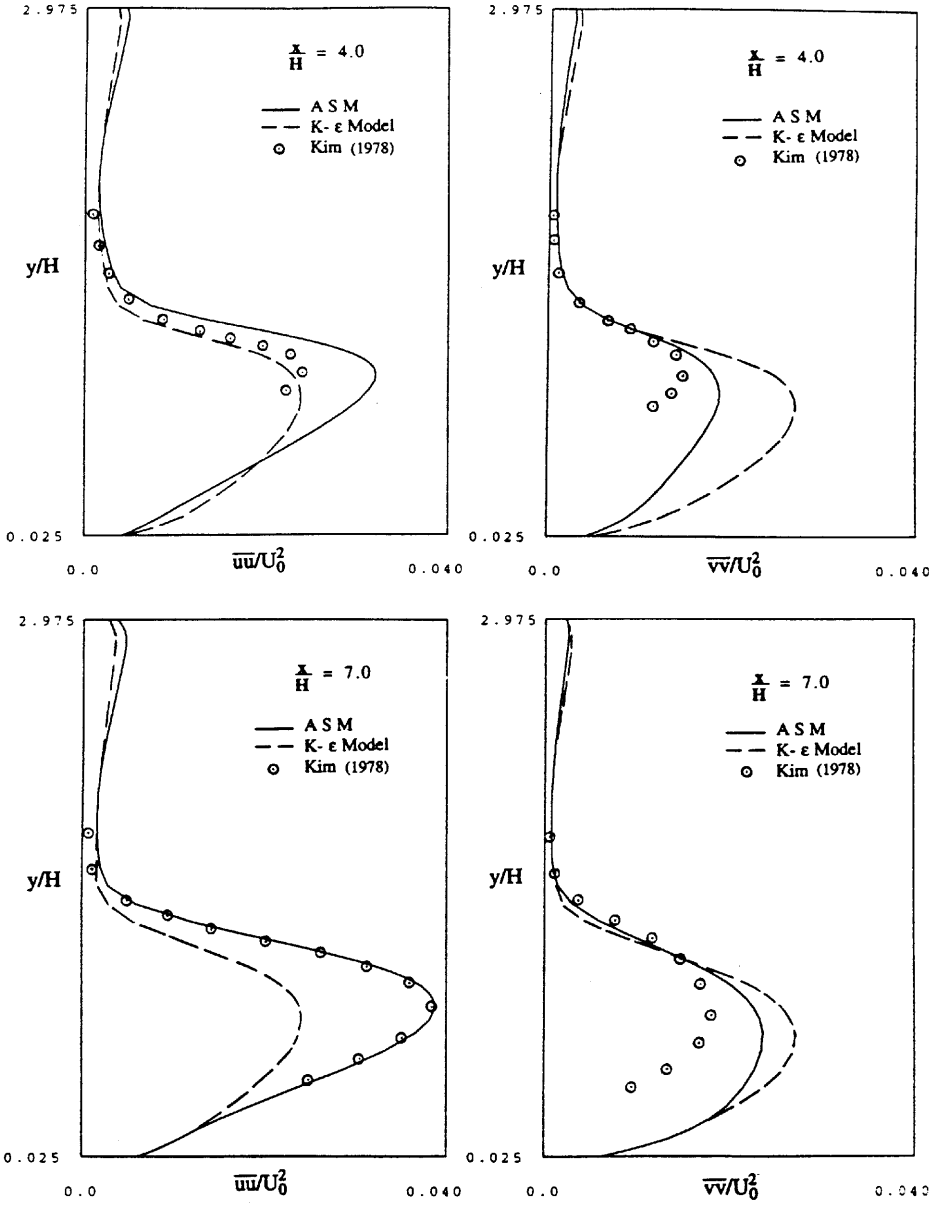

Figure 12. Comparison of normal Reynolds stresses at x/H of 4·0 and 7·0 downstream of step. The maximum inlet velocity is U_0 and H is the step height. The experimental data are taken from Reference 16

Flow around a box

The two-dimensional turbulent flow around a square cylinder or box is an intrinsically transient problem in which vortices are alternately shed from the forward corners; the dominant shedding frequency f is usually stated in terms of the Strouhal number $S = fH/U_0$. The technical literature abounds with computations of laminar flow around a box, but only Franke and Rodi[21] and

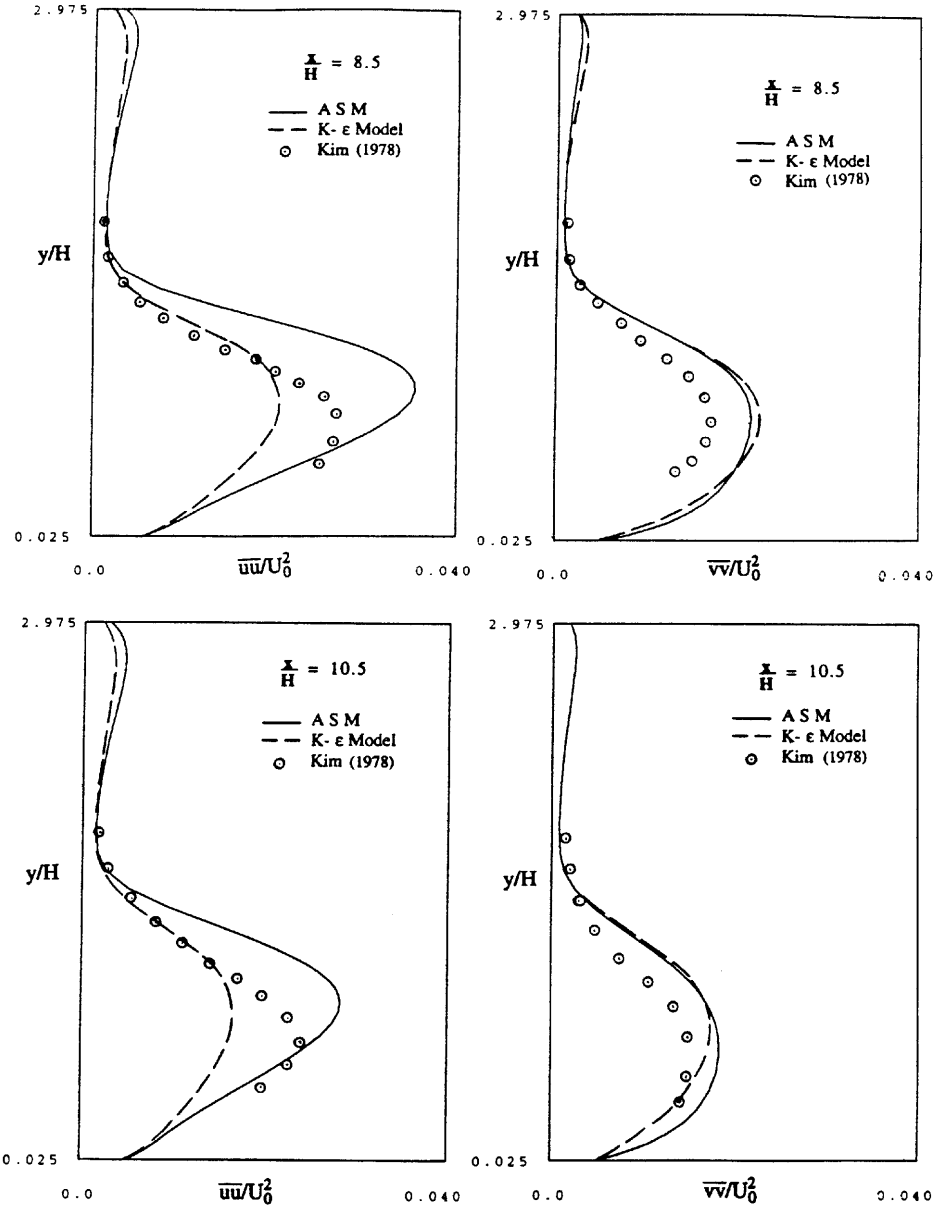

Figure 13. Comparison of normal Reynolds stresses at x/H of 8·5 and 10·5 downstream of step. The maximum inlet velocity is U_0 and H is the step height. The experimental data are taken from Reference 16

Haroutunian[22] appear to have computed the turbulent flow about a box. Also, some work appears to have been done in the laboratory; notable experiments have been reported by Durão *et al.*[23] and Okajima.[24]

This problem was first studied with a relatively coarse 2200-element mesh and results were obtained for the $K-\varepsilon$ model and the ASM. To confirm the early results, to learn something of the

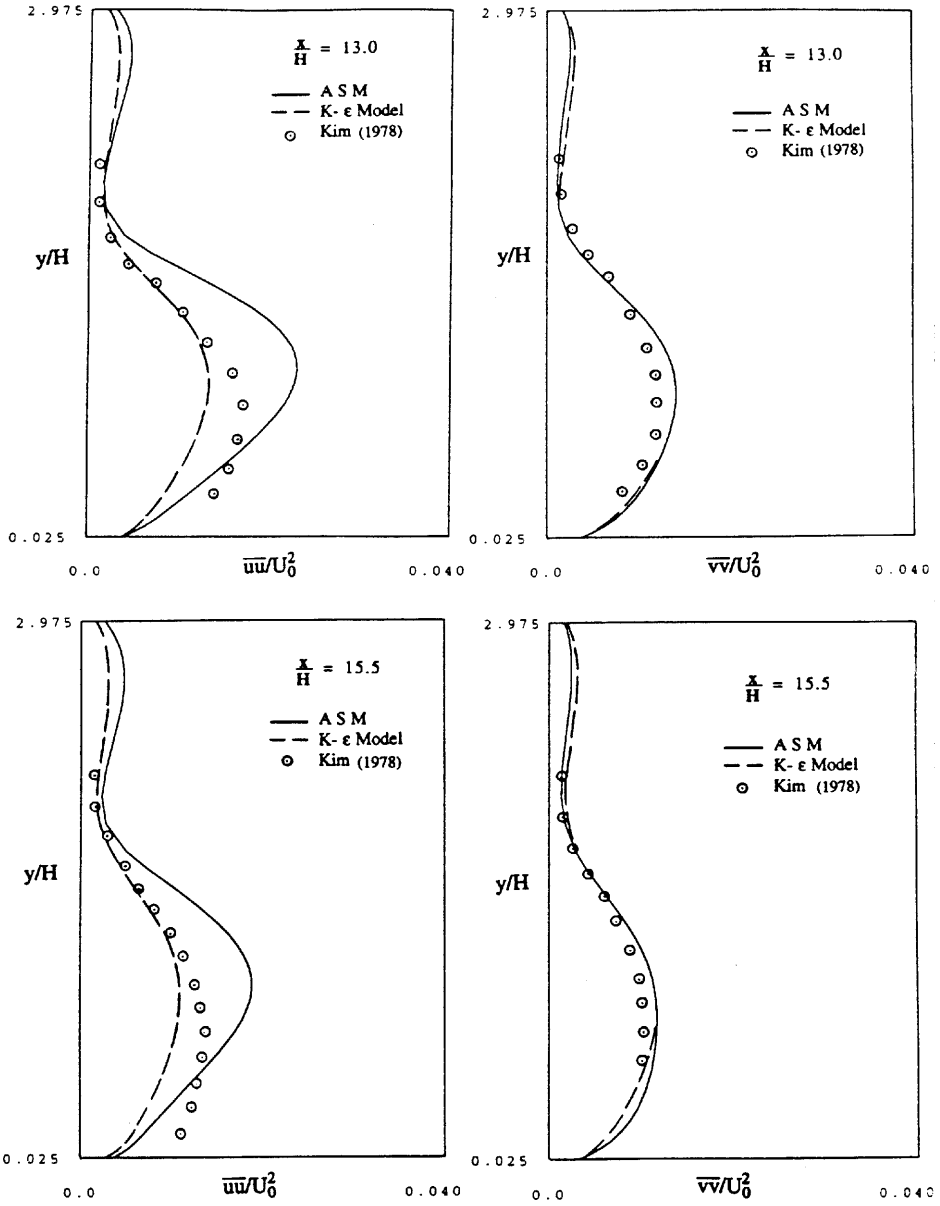

Figure 14. Comparison of normal Reynolds stresses at x/H of 13·0 and 15·5 downstream of step. The maximum inlet velocity is U_0 and H is the step height. The experimental data are taken from Reference 16

effect of further mesh refinement and to produce smoother plots, a 4004-element mesh, was also used for the ASM. In each case the domain was 10 by 20 box heights H ($-5{\cdot}0 \leqslant x/H \leqslant 15{\cdot}0$ and $-5{\cdot}0 \leqslant y/H \leqslant 5{\cdot}0$), which is similar to the 14 by 20 domain used by Franke and Rodi.[21] For comparison purposes the chosen Reynolds number was 23,500 based on $U_0 = 2{\cdot}35$ m s^{71} and $H = 0{\cdot}1$ m; in addition $y_n/H = 0{\cdot}05$ was used. Figure 16 shows the finer mesh and lists boundary

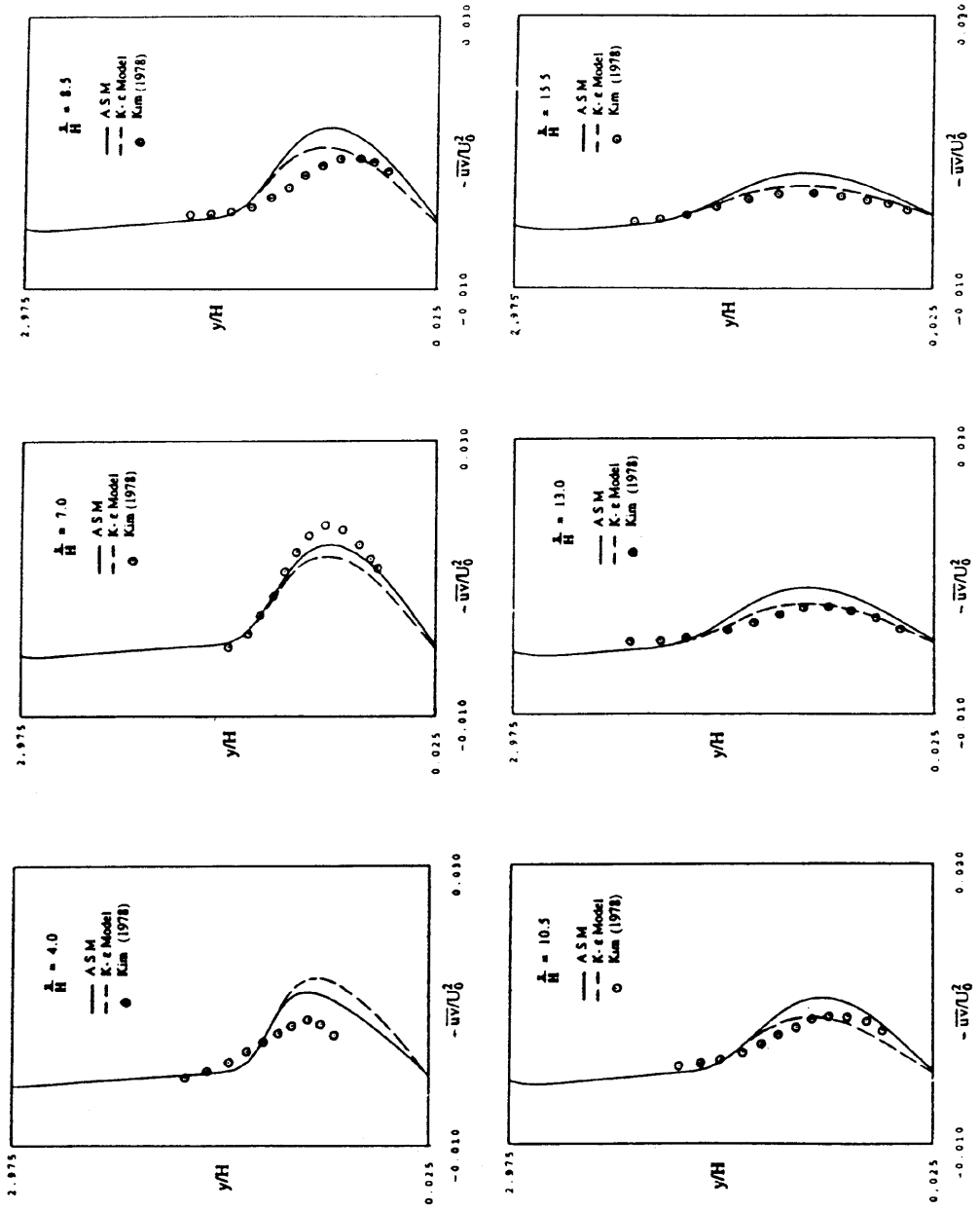

Figure 15. Reynolds shear stress profiles predicted by ASM and $K-\varepsilon$ models compared with Kim's[16] experimental data

conditions on it. Franke and Rodi[21] indicate that special wall functions were needed to initiate the shedding of vortices. Here on the box surfaces the wall law given in equation (18) was applied without alteration, and normal mean velocities were zero, including the corners of the box. The remaining boundary conditions for this problem are shown in Figure 16.

The $K-\varepsilon$ model on the course mesh was initialized and run for a time interval which was shorter than that required to begin shedding vortices (the initial shedding time is about 6 s); the outcome of this run was used to initialize all subsequent computations. The $K-\varepsilon$ computations simply continued from this start. The ASM computations continued on the coarse mesh and were regularly shedding vortices by 6·0 s. The ASM computations on the finer mesh were started from the coarse mesh result at 6·0 s.

Figure 17 is the streamline pattern from the finer mesh at a time of 7 s; this data set was compared with $K-\varepsilon$ and ASM results from the coarser mesh. For this flow Okajima[24] found the Strouhal number to be 0·12–0·13. From this fine mesh the Strouhal number was 0·11, while the $K-\varepsilon$ model on the coarse mesh yielded 0·10 and the ASM on the coarse mesh gave the closest prediction at 0·13. For detail on determination of the Strouhal number for a flow, see Gresho *et al.*[25] A streamline plot based on the coarse mesh would possess the same features as Figure 17 but would be more angular.

Contours of normalized turbulence kinetic energy K/U_0^2 are presented in Figure 18. A small zone of high energy which appeared with the vortex in the coarse grid does not appear here, but three other zones of locally high energy can still be seen. Some clipping is used to keep the energy at these points within reasonable bounds; the clipping process was never applied at more than 113 of the 4000 nodes and the average contour number involved was about 50 nodes, mostly at points in the wake region. Not surprisingly, a plot for the dissipation rate is very similar in form to this figure. Similar results for both variables were obtained for both models on the coarse mesh.

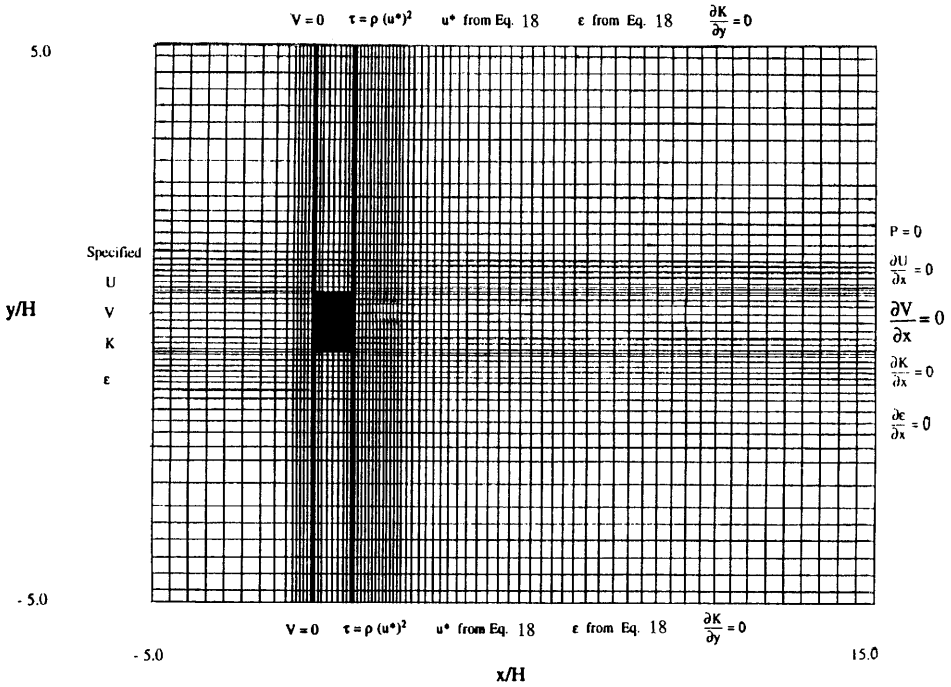

Figure 16. Computational mesh and boundary conditions for 4004-element model of flow around box

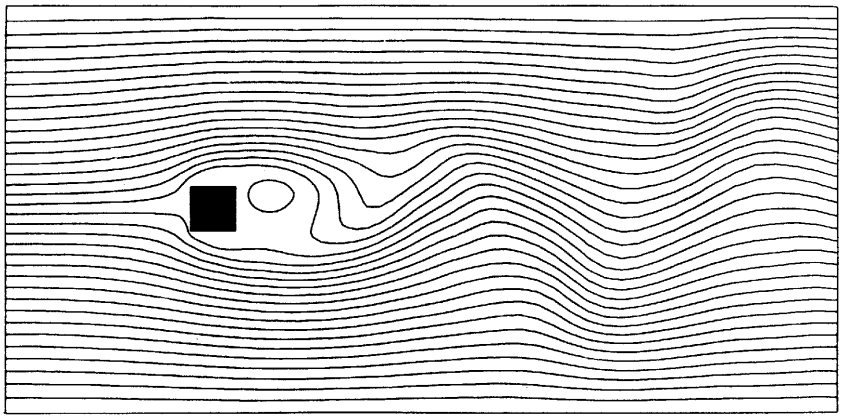

Figure 17. Streamlines predicted by 4004-element ASM for turbulent flow around box at Reynolds number 23,500 at time 7 s

A pair of contour plots for the normalized normal Reynolds stresses $\overline{uu}/U_0^2$ and $\overline{vv}/U_0^2$ is presented in Figures 19 and 20. The stress distributions are similar but by no means identical. For the interested reader Ross[9] presents over 40 additional plots of results for this problem.

CONCLUSIONS

The present finite element model of transient turbulent flow has done well in several benchmark tests of its ability to simulate fully developed flow in channels, the flow past a backward-facing step and the flow past a square box. Consequently, this computational scheme deserves full consideration as a viable computational method for implementation in the computation of three-dimensional transient turbulent flows.

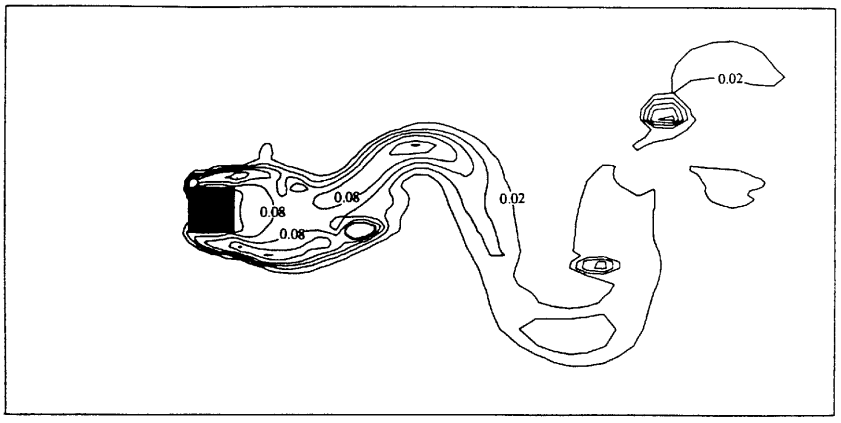

Figure 18. Contour plot of non-dimensional turbulence kinetic energy per unit mass, K/U_0^2, contour interval 0·02, for 4004-element ASM of turbulent flow around box

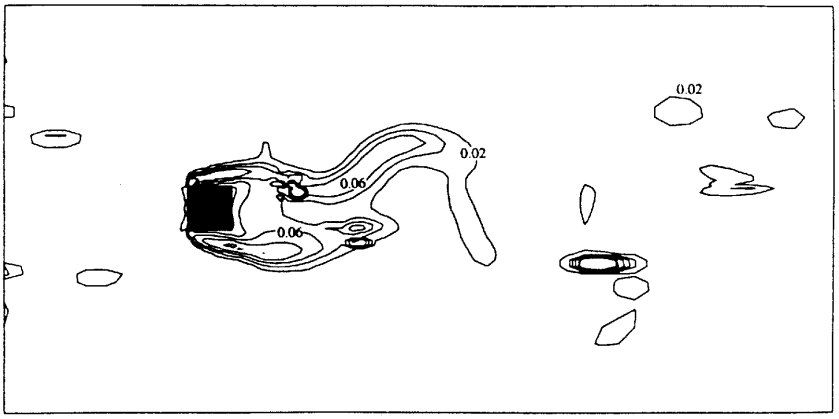

Figure 19. Contour plot of non-dimensional normal Reynolds stress $\overline{uu}/U_0^2$, contour interval 0·02, for 4004-element ASM of turbulent flow around box. The maximum value is about 0·10 at the leading corners of the box

The initialization procedures for the computational scheme performed well. The balancing tensor diffusivity terms appear to compensate well for the numerical diffusion that is a part of using the explicit forward Euler time integration. The novel but infrequently required 'clipping' of some source terms appears to be a simple but successful way to stabilize computations in the algebraic stress model portion of the method.

In the comparisons that could be made with the results of other computations or with experimental data, whether they be mean flow streamline patterns or separation lengths or the distribution of various turbulence parameters, or in the comparison of computed Strouhal numbers with experiment for the shedding of vortices from the box, the results from this numerical model appear to meet or exceed in accuracy the results of most other computations.

Shortly after the computations reported herein were completed, Gatski and Speziale[26] published a new explicit ASM and also commented on the history and causes of problems in using implicit

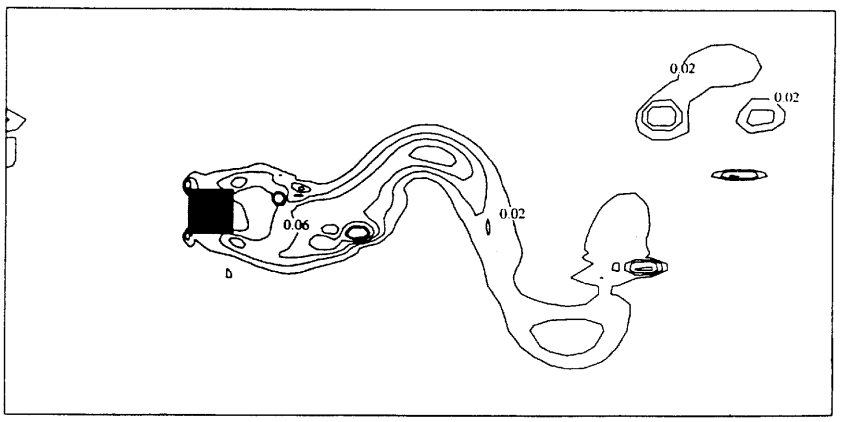

Figure 20. Contour plot of non-dimensional normal Reynolds stress $\overline{vv}_0^2$, contour interval 0·02, for 4004-element ASM of turbulent flow around box. The maximum value is about 0·08 at the leading corners of the box

models. Their model is made explicit by the use of integrity basis functions from linear algebra and Mathematica^{TM} to do the actual algebra.[27] Their model is certainly elegant in comparison with the simple strategem of clipping. In the future one would expect to see the explicit model used in many computations if the effort of implementing it is not a deterrent. On the other hand, the simple, unsophisticated strategy of clipping may also receive some attention in future research and continue to be a useful tool.

ACKNOWLEDGEMENTS

R. L. Lee made arrangements for J. A. Ross to work at Lawrence Livermore National Laboratory, California, and helped him get started on the research. Others who also assisted in one way or another at LLNL are P. M. Gresho, J. M. Leone Jr., S. T. Chan, R. McCallen and R. Cederwall. We appreciate their help.

1. W. Rodi, *Turbulence Models and their Application in Hydraulics—A State of the Art Review*, IAHR, Delft, 1980.
2. W. Rodi, 'A new algebraic relation for calculating the Reynolds stresses', *ZAMM*, **56**, T219–T221 (1976).
3. C. G. Speziale, 'On nonlinear k–l and k–ε models of turbulence', *J. Fluid Mech.*, **178**, 459–475 (1987).
4. G. Ahmadi and S. J. Chowdhury, 'A rate-dependent algebraic stress model for turbulence', *Appl. Math. Model.*, **15**, 516–524 (1991).
5. B. E. Launder, 'On the effect of a gravitational field on the turbulent transport of heat and momentum', *J. Fluid Mech.*, **67**, 569–581 (1975).
6. C. G. Speziale and T. Ngo, 'Numerical solution of turbulent flow past a backward facing step using a nonlinear $k-\varepsilon$ model', *Int. J. Eng. Sci.*, (10), 1099–1112 (1988).
7. P. M. Gresho, S. T. Chan, R. L. Lee and C. D. Upson, 'A modified finite element method for solving the time-dependent, incompressible Navier–Stokes equations. Part 1: Theory', *Int. j. numer. methods fluids*, **4**, 557–598 (1984).
8. V. A. Haroutunian, 'Time-dependent finite element model for atmospheric dispersion of gases heavier than air', *Ph.D. Thesis*, University of Manchester, 1987.
9. J. A. Ross, 'An algebraic stress finite element model for recirculating turbulent flows', *Ph.D. Thesis*, University of California, Davis, CA, 1993.
10. J. A. Ross and B. E. Larock, 'Developing an algebraic stress finite element model of turbulent flow', in M. Cecchi *et al.* (eds), *Proc. IX Int. Conf. on Finite Elements in Fluids: New Trends and Applications*, Venice, October 1995, Part I, pp. 667–676.
11. D. R. Schamber, 'Finite element analysis of flow in sedimentation basins', *Ph.D. Thesis*, University of California, Davis, CA, 1979.
12. J. Laufer, 'Investigation of turbulent flow in a two-dimensional channel', *NACA Rep. 1053*, 1951, pp. 1247–1266.
13. J. A. Clark, 'A study of incompressible turbulent boundary layers in channel flow', *J. Basic Eng., ASME*, **90**, 455–468 (1968).
14. A. K. M. F. Hussain and W. C. Reynolds, 'Measurements in fully developed turbulent channel flow', *J. Fluids Eng.*, ASME, **97**, *569–580 (1975).*
15. D. R. Schamber and B. E. Larock, 'Computational aspects of modeling turbulent flows by finite elements', in K. Morgan *et al.* (eds), *Computer Methods in Fluids*, Pentech, London, 1980, pp. 339–361.
16. J. S. Kim, 'Investigation of separation and reattachment of a turbulent shear layer: flow over a backward-facing step', *Ph.D. Thesis*, Stanford University, Stanford, CA, 1978.
17. P. L. Betts and V. A. Haroutunian, 'k–ε modeling of turbulent flow over a backward-facing step by a finite element method; comparison with finite volume solutions and experiment', in C. Taylor *et al.* (eds), *Numerical Methods in Laminar and Turbulent Flow*, Pineridge, Swansea, 1985.
18. S. Thangam and C. G. Speziale, 'Turbulent flow past a backward-facing step, a critical evaluation of two-equation models', *AIAA J.*, **30**, 1314–1320 (1992).
19. R. L. Lee, 'A finite element/finite difference approach for modeling three-dimensional flow and pollutant dispersion around structures', *LLNL Preprint UCRL-JC-107758 R1*, 1992.
20. J. K. Eton, 'Turbulent flow reattachment: an experimental study of the flow and structure behind a backward-facing step', *Ph.D. Thesis*, Stanford University, Stanford, CA, 1980.
21. R. Franke and W. Rodi, 'Calculation of vortex shedding past a square cylinder with various turbulence models', in F. Durst *et al.* (eds), *Turbulent Shear Flows 8: Selected Papers from Eighth Int. Symp. of Turbulent Shear Flows*, Munich, September 1991, Springer, Berlin, 1991.
22. V. A. Haroutunian, personal communication, 1990.

23. D. F. G. Durão, M. V. Heitor and J. C. F. Periera, 'Measurements of turbulent and periodic flows around a square cross-section cylinder', *Exp. Fluids* **6**, 298–304 (1988).
24. A. Okajima, 'Strouhal numbers of rectangular cylinders', *J. Fluid Mech.*, **123**, 379–398 (1982).
25. P. M. Gresho, R. L. Lee and R. L. Sani, 'On the time dependent solution of the incompressible Navier–Stokes equations in two and three dimensions', in C. Taylor and K. Morgan (eds), *Recent Advances in Numerical Methods in Fluids*, Vol. 1, Pineridge, Swansea, 1980.
26. T. B. Gatski and C. G. Speziale, 'On explicit algebraic stress models for complex turbulent flows', *J. Fluid Mech.*, **254**, 59–78 (1993).
27. S. Wolfram, *Mathematica*, Addison-Wesley, New York, 1988.

